Cell Death and Differentiation (2015) 22, 1687–1699

www.nature.com/cdd

The small GTPase Rab29 is a common regulator of immune synapse assembly and ciliogenesis

A Onnis[1], F Finetti[1], L Patrussi[1], M Gottardo[1], C Cassioli[1], S Spanò[2] and CT Baldari*[,1]

Accumulating evidence underscores the T-cell immune synapse (IS) as a site of intense vesicular trafficking, on which productive signaling and cell activation crucially depend. Although the T-cell antigen receptor (TCR) is known to exploit recycling to accumulate to the IS, the specific pathway that controls this process remains to be elucidated. Here we demonstrate that the small GTPase Rab29 is centrally implicated in TCR trafficking and IS assembly. Rab29 colocalized and interacted with Rab8, Rab11 and IFT20, a component of the intraflagellar transport system that regulates ciliogenesis and participates in TCR recycling in the non-ciliated T cell, as assessed by co-immunoprecipitation and immunofluorescence analysis. Rab29 depletion resulted in the inability of TCRs to undergo recycling to the IS, thereby compromizing IS assembly. Under these conditions, recycling TCRs accumulated in Rab11$^+$ endosomes that failed to polarize to the IS due to defective Rab29-dependent recruitment of the dynein microtubule motor. Remarkably, Rab29 participates in a similar pathway in ciliated cells to promote primary cilium growth and ciliary localization of *Smoothened*. These results provide a function for Rab29 as a regulator of receptor recycling and identify this GTPase as a shared participant in IS and primary cilium assembly.
Cell Death and Differentiation (2015) **22,** 1687–1699; doi:10.1038/cdd.2015.17; published online 13 March 2015

T-cell activation is triggered by T-cell antigen receptor (TCR) engagement by MHC-bound peptide dispayed by an antigen presenting cell (APC). While a substantial proportion of the TCR has long been known to be associated with recycling endosomes,[1] it is only recently that the central function of this pool has emerged with the finding that, on assembly of the specialized interface with the APC, known as the immune synapse (IS), intracellular TCRs are delivered to this location by polarized recycling.[2] This process ensures a steady supply of TCRs at the IS to sustain signaling for T-cell activation[3] and has been co-opted by other receptors, such as the transferrin receptor (TfR) and the chemokine receptor CXCR4,[4,5] as well as membrane-bound signaling mediators, such as the kinase Lck and the adaptor LAT.[6,7]

Receptor recycling is orchestrated by the small GTPases Rab4 and Rab11.[8] Cargo specificity is achieved with the assistance of specific regulators and effectors. The TCR recycling pathway has only started to be delineated with the identification of specific mediators, which include Rab35 and its GAP EPI64C[9] and the actin adaptor WASH[10]. Specific combinations of Rabs and SNAREs have been recently associated with recycling endosomes carrying either Lck, or TCRζ and LAT.[11] We have moreover identified IFT20[12] and other components of the intraflagellar transport (IFT) system, which regulates ciliary assembly and function,[13] as unexpected regulators of TCR recycling in the non-ciliated T cell.[14]

Recently a Rab GTPase subfamily, which includes Rab29, Rab32 and Rab38, has been implicated in trafficking of the *Salmonella*-containing vacuole (SCV) in infected epithelial cells.[15,16] Rab32 and Rab38 participate in the generation and traffic of melanosomes,[17] while Rab29 regulates retrograde endolysosome-to-Golgi trafficking of the mannose-6-phosphate receptor (MPR) in epithelial and neuronal cells.[18,19] Based on the implication of Rab29 in typhoid toxin trafficking to the plasma membrane from the SCV,[15] where Rab4 and Rab11 have also been observed,[20] here we assessed the role of Rab29 in the regulation of TCR recycling. The results identify Rab29 as a novel regulator of vesicular trafficking in T cells, acting as a complex with IFT20 and the Rabs Rab8 and Rab11 to control TCR recycling and IS assembly. We also show that Rab29 participates in a similar pathway to control primary cilium growth and the ciliary localization of the receptor *Smoothened*, undescoring the homologies between cilium and IS.

Results

Rab29 colocalizes and interacts with Rab8, Rab11 and IFT20 in T cells. Rab29 was found to be expressed in peripheral blood T cells as well as Jurkat T cells, as assessed by real-time PCR and immunoblot (Figures 1a and b). At variance, low levels of Rab32 and Rab38 mRNA were detectable in these cells (Figure 1a). Hence subsequent analyses were focused on Rab29.

The localization of Rab29 was analyzed in T cells transiently transfected with a plasmid encoding GFP-tagged Rab29.

[1]Department of Life Sciences, University of Siena, 53100 Siena, Italy and [2]School of Medical Sciences, University of Aberdeen, Aberdeen AB25 2ZD, UK
*Corresponding author: CT Baldari, Department of Life Sciences, University of Siena, Via Aldo Moro 2, Siena 53100, Italy. Tel: +39 577 234400; Fax: +39 577 234476; E-mail: cosima.baldari@unisi.it

Abbreviations: APC, antigen presenting cell; esiRNA, endoribonuclease-prepared siRNA; GFP, Green Fluorescent Protein; IFT, intraflagellar transport; IS, immune synapse; MPR, mannose-6-phosphate receptor; RAB, Ras-related protein; RLUC, Renilla Luciferase; RNAi, RNA interference; Sag, Superantigen; SCV, *Salmonella*-containing vacuole; SEB, Staphylococcal enterotoxin B; SEE, Staphylococcal enterotoxin E; SEM, Scanning Electron Microscope; Smo, Smoothened; TCR, T-cell antigen receptor; TGN, trans-Golgi network; TEM, Transmission Electron Microscope; TfR, Transferrin receptor

Received 09.11.14; revised 21.1.15; accepted 02.2.15; Edited by L Zitvogel; published online 13.3.15

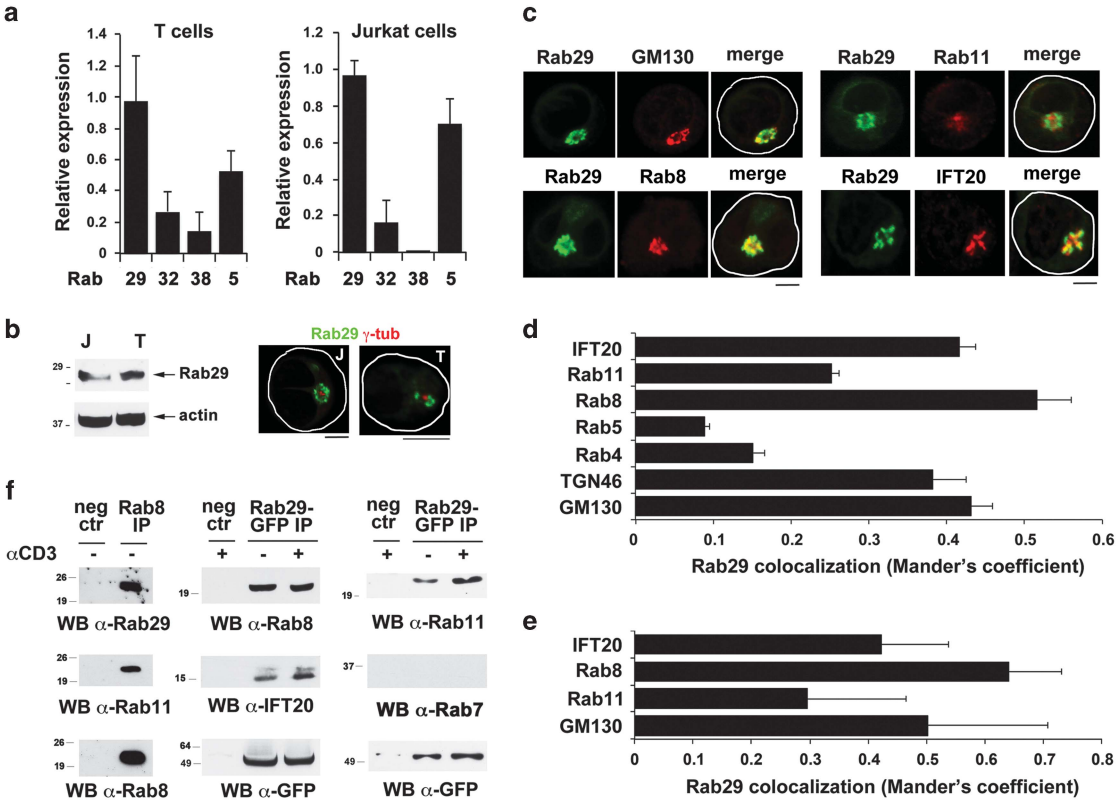

Figure 1 Rab29 is expressed in T cells and associates with Rab8, Rab11 and IFT20. (**a**) Relative expression of Rab29, Rab32 and Rab38 mRNA in human T cells, as determined by real-time RT-PCR. Rab5 was included as an ubiquitous Rab control. The data, determined on triplicate samples using the ddCt method, are expressed using Rab29 as a reference. Error bars, S.D. ($n \geq 3$). (**b**) *Left*, Immunoblot analysis of Rab29 in lysates of Jurkat (J) and T cells ($n \geq 3$). *Right*, Immunofluorescence analysis of Rab29 in Jurkat and T cells transiently transfected with construct encoding GFP-tagged Rab29 (green) costained with an anti-γ-tubulin mAb (red). (**c**–**e**) Quantification (mean ± S.D.) using Mander's coefficient of the weighted colocalization of GFP with the indicated vesicular markers in the GFP-tagged Rab29 Jurkat transfectant (**d**) or primary T cells transiently transfected with the GFP-tagged Rab29 construct (**e**). At least 20 Jurkat cells and 10 T cells were analyzed for each marker ($n \geq 3$). Representative images (medial optical sections) are shown (**c**). Size bar, 5 μm. (**f**) *Left*, Immunoblot analysis of Rab8-specific immunoprecipitates from Jurkat cell lysates. *Middle, right*, Immunoblot analysis of GFP-specific immunoprecipitates from lysates of GFP-Rab29-expressing Jurkat cells, either unstimulated or activated for 10 min by TCR cross-linking. Preclearing controls (proteins that bound to Protein-A–Sepharose before the addition of primary antibody) are included in each blot (neg ctr). The migration of molecular mass markers is indicated. Total cell lysates were included in each gel to identify the migration of the proteins tested. The immunoblots shown are representative of three independent experiments

Rab29 staining was largely limited to a vesicular pericentrosomal compartment (Figure 1b). Immunofluorescence analyses on GFP-Rab29-expressing cells showed that Rab29 colocalizes with GM130 (cis-Golgi) and TGN46 (trans-Golgi network), similar to epithelial cells.[15,18,19] Rab29 also colocalized with Rab11, while a limited colocalization was observed with both Rab4 (recycling endosomes) and Rab5 (early endosomes) (Figures 1c–e). Based on our findings implicating IFT20 in TCR recycling[5,14] as well as on the association of TCRζ with Rab8[11] which is similar to IFT20 is implicated in ciliogenesis,[21] the colocalization of Rab29 with these proteins was assessed. Rab29 strongly colocalized with both Rab8 and IFT20 (Figures 1c–e), suggesting its implication in the recycling pathways controlled by these trafficking regulators in T cells.

The ability of Rab29 to interact with Rab8, Rab11 and IFT20 was assessed in co-immunoprecipitation experiments on GFP-Rab29-expressing Jurkat cells, either unstimulated or activated by TCR ligation. Both Rab8 and Rab11, but not Rab7 (late endosomes), were found to constitutively form a complex with Rab29. An interaction of IFT20 with Rab29, which was enhanced following TCR triggering, was also observed (Figure 1f). Since IFT20 interacts with the TCR at early endosomes, promoting its transit to recycling endosomes,[5] the results suggest that Rab29 participates together with Rab8 in the Rab11-dependent pathway of TCR recycling downstream of IFT20.

Rab29 controls TCR recycling. The role of Rab29 in TCR recycling was addressed using a tool GtgE, a type-III secretion effector that broad-host *Salmonella* serovars use to modulate SCV trafficking by specifically cleaving Rab29, Rab32 and Rab38.[15,16] Since neither Rab32 nor Rab38 is expressed at significant levels in T cells, GtgE can be used to specifically deplete Rab29. Jurkat T-cell transfection with a GtgE expression construct resulted in the expected reduction of endogenous Rab29 (Figure 2a). This was reflected by a dispersion of the compact GFP-Rab29 staining (Supplementary Figure S1A). Although the GPF cleavage product lacks the Rab29 membrane localization sequence,[15] staining appeared particulate rather than diffuse, likely resulting from aggregation of the truncated protein. Rab29 depletion did not affecting either cell viability (Supplementary Figure S1B) or expression of its interactors (Supplementary

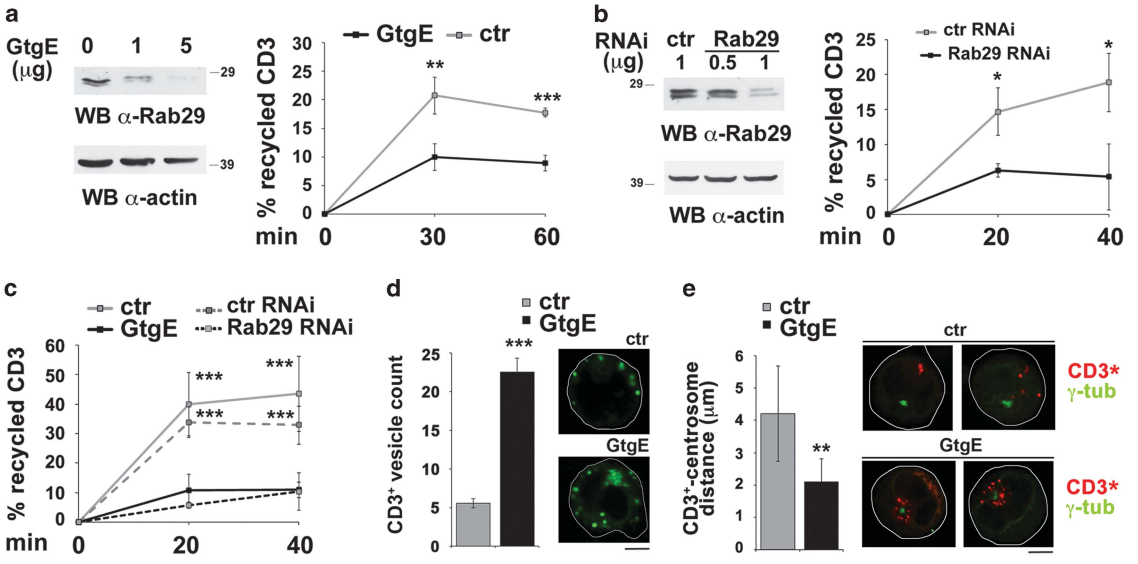

Figure 2 Rab29 is required for TCR recycling. (**a**) *Left*, Anti-Rab29 immunoblot of lysates of Jurkat cells either untransfected or transfected with different amounts of a plasmid encoding GtgE (residual Rab29, normalized to actin: 5 μg, 62.5%; 1 μg, 22.2%). *Right*, Flow cytometric analysis of TCR recycling in the control and GtgE-expressing stable Jurkat transfectants (Rab29 depletion ~60%). The data, which for each time point refers to triplicate samples from three independent experiments, are presented as % of internalized receptors that have recycled to the cell surface. (**b**) *Left*, Anti-Rab29 immunoblot of lysates of control and Jurkat cells transfected with different amounts of Rab29 siRNA (residual Rab29: 0.5 μg, 39.6%; 1 μg, 81.5%). *Right*, Flow cytometric analysis of TCR recycling in control and Rab29KD Jurkat cells (Rab29 depletion ~70%). Each time point refers to triplicate samples from three independent experiments. (**c**) Flow cytometric analysis of TCR recycling in control and GtgE-expressing transient peripheral blood T-cell transfectants (Rab29 depletion ~50%), or control and Rab29KD primary T cells (Rab29 depletion >50%). Each time point refers to duplicate samples from at least three donors. The significance refers to the ctr/GtgE and ctr RNAi/Rab29RNAi pairs. (**d**) Counts of vesicles containing internalized CD3 in control and GtgE-expressing Jurkat cells. The data are presented as the number of labeled vesicles in individual medial confocal sections. At least 60 cells were analyzed for each marker ($n \geq 3$). (**e**) Quantification of the distance (mean ± S.D.) of vesicles containing internalized CD3 (CD3*, red) from the centrosome (green) in control and GtgE-expressing Jurkat cells co-stained for γ-tubulin. At least 25 cells were analyzed for each transfectant ($n = 3$). Representative images are shown. Size bar, 5 μm. Error bars, S.D. ***$P < 0.001$; **$P < 0.01$; *$P < 0.05$

Figure S1C). No obvious alteration in either the Golgi or the recycling compartment or in IFT20 localization was observed (Supplementary Figure S1D).

The impact of GtgE-mediated Rab29 depletion on TCR recycling was assessed using Jurkat cells stably transfected with the GtgE-encoding construct. TCR internalization was induced using a specific mAb. Internalized receptors were then allowed to recycle to the cell surface, where they were tracked by flow cytometry using fluorochrome-labeled secondary antibodies. While not affecting TCR expression or internalization (Supplementary Figures S2A and B), Rab29 depletion resulted in a severe impairment in TCR recycling (Figure 2a). Similar results were obtained when Rab29 was depleted by RNA interference (RNAi) to rule out off-target effects of GtgE (Figure 2b). The results were confirmed on primary T cells (Figure 2c). As a complementary approach, internalized TCRs were tracked by confocal microscopy in permeabilized cells. Consistent with the TCR recycling defect, Rab29 depletion resulted in the accumulation of TCR^+ endosomes around the centrosome (Figures 2d and e).

The analysis was extended to the TfR and CXCR4, which also undergo constitutive as well as polarized recycling to the IS.[4,5] No effect was observed on TfR recycling (Supplementary Figures S2A, B, S3A, B and E) while, similar to the TCR, Rab29 depletion resulted in a defect in CXCR4 recycling (Supplementary Figures S2A, B, S3C, D and F). Hence Rab29 is a selective regulator of receptor recycling in T cells.

Rab29 controls polarized TCR recycling to the IS and downstream signaling. To address the role of Rab29 in polarized TCR recycling, the localization of Rab29 was first analyzed in conjugates of GFP-Rab29-expressing Jurkat cells with Staphylococcal enterotoxin-E (SEE)-loaded Raji cells used as APC. Rab29 polarized to the IS together with endosomal TCR and the centrosome (Figures 3a and b). Under these conditions, a significant colocalization of internalized TCRs with GFP-Rab29 was observed (Figure 3c), suggesting a role for Rab29 in polarized TCR recycling.

To address this issue, TCRs that had been internalized at the cell surface were tracked in antigen-specific conjugates of control and Rab29-depleted Jurkat cells stained with secondary antibodies without prior permeabilization. Under these conditions, only receptors that have recycled can be visualized. Delivery of internalized TCRs to the IS membrane was significantly impaired in cells depleted of Rab29 either by GtgE expression or by RNAi, as assessed by measuring the proportion of conjugates harboring CD3 staining at the APC contact (Figures 3d and e). The results were confirmed on primary T cells (Figure 3h). Rab29 depletion did not affect polarized TfR recycling (Supplementary Figures S4A, B and E) while compromizing CXCR4 recycling to the IS (Supplementary Figures S4C, D and F). Moreover, the overall IS polarization of the $Rab11^+$ compartment was not significantly affected by Rab29 depletion (Supplementary Figure S4, legend), supporting the selective function of Rab29 in receptor recycling.

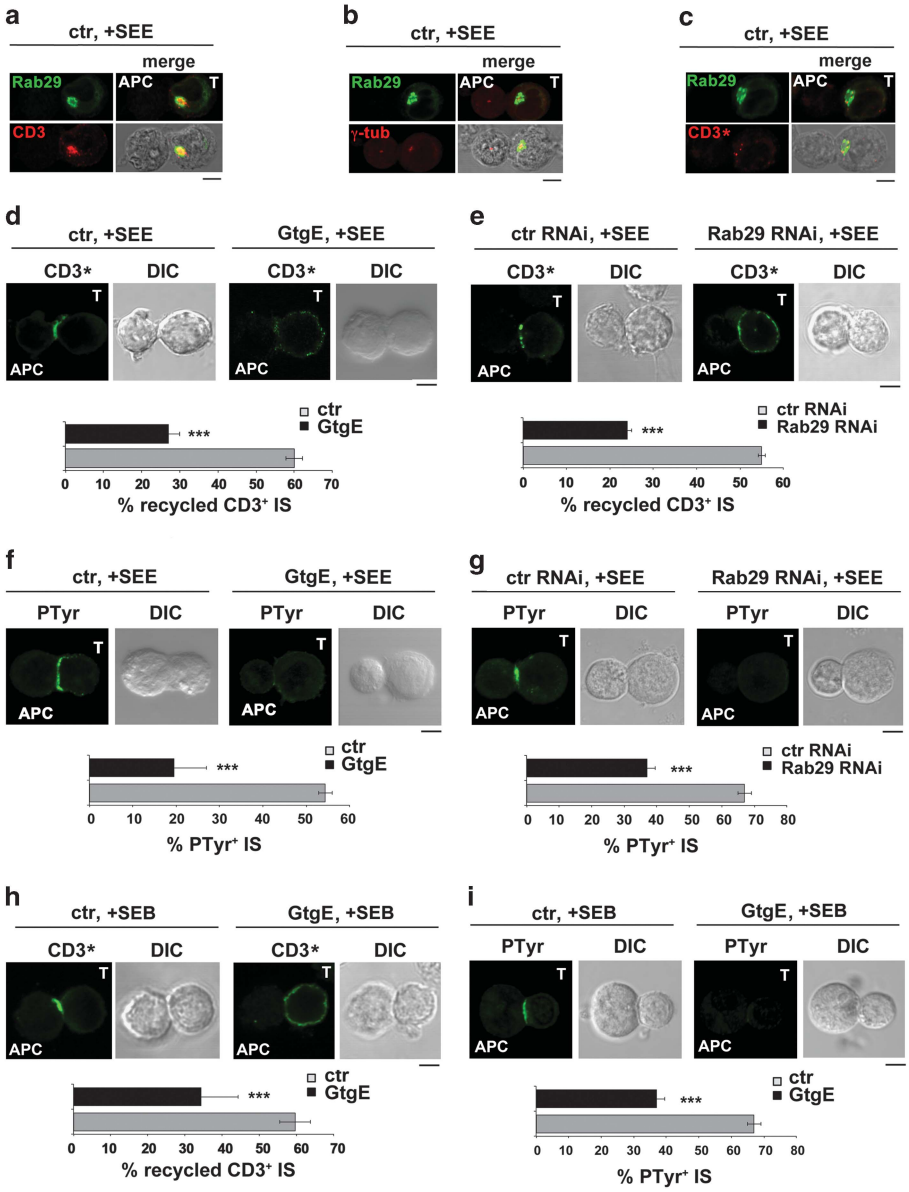

Figure 3 Rab29 is required for the polarization of TCR recycling to the IS and downstream signaling. (**a**) Immunofluorescence analysis of CD3 (red) (**a**) or γ-tubulin (red) (**b**) localization in conjugates of Jurkat cells expressing GFP-tagged Rab29 (green) and SEE-pulsed Raji cells (APC). Mander's coefficient of the weighted colocalization of the $CD3^+$ vesicles (red) in the $Rab29^+$ compartment (green) in individual medial confocal sections of at least 20 cells was 0.52 ± 0.15. (**c**) Immunofluorescence analysis of recycling CD3 ($CD3^*$, red) in permeabilized GFP-Rab29 (green)-expressing Jurkat cells conjugated with SEE-pulsed Raji cells (APC). Mander's coefficient of the weighted colocalization of the $CD3^+$ vesicles (red) in the $Rab29^+$ compartment (green) in individual medial confocal sections of at least 20 cells was 0.36 ± 0.14 ($n = 3$). (**d**, **e**, **h**) Immunofluorescence analysis under non-permeabilizing conditions of recycled CD3 ($CD3^*$) on control or GtgE-expressing Jurkat cells (**d**) or primary T cells (**h**), and control or Rab29KD Jurkat cells (**e**), conjugated with SEE/SEB-pulsed Raji cells (APC). Quantifications (%) of conjugates with recycled CD3 at the IS are shown below the representative images. At least 20 cells were analyzed in each experiment ($n \geq 3$). (**f**, **g**, **i**) Immunofluorescence analysis of tyrosine phosphoproteins (PTyr) in conjugates of control and GtgE-expressing Jurkat cells (**f**) or primary T cells (**i**), or control and Rab29KD Jurkat cells (**g**), and SEE/SEB-pulsed Raji cells (APC). Quantification (%) of conjugates with PTyr staining at the IS is shown below the representative images. At least 300 cells were analyzed for each marker ($n \geq 3$). Size bar, 5 μm. Error bars, S.D. $^{***}P < 0.001$

Consistent with the failure of recycling TCRs to effectively concentrate at the IS, signaling was impaired in Rab29-depleted cells, as shown by staining with anti-phosphotyrosine mAb (Figures 3f, g and i). Of note, effective protein tyrosine phosphorylation was observed at the onset on IS assembly in GtgE-expressing cells (Figure 4a), indicating that TCR signaling was initiated normally but was not sustained in the absence of Rab29, consistent with the defective IS delivery of endosomal TCRs. This was confirmed by a time course analysis of Erk phosphorylation (Figure 4b). The defective activation of the tyrosine phosphorylation cascade in Rab29-depleted T cells resulted in impaired cell activation by SAg-loaded APC, as shown by measuring CD69 and IL-2 expression (Figures 4c–e). Hence Rab29 participates in T-cell activation by controlling polarized TCR recycling to the IS.

Rab29 regulates receptor recycling downstream of Rab11 by interacting with molecular motors. To identify

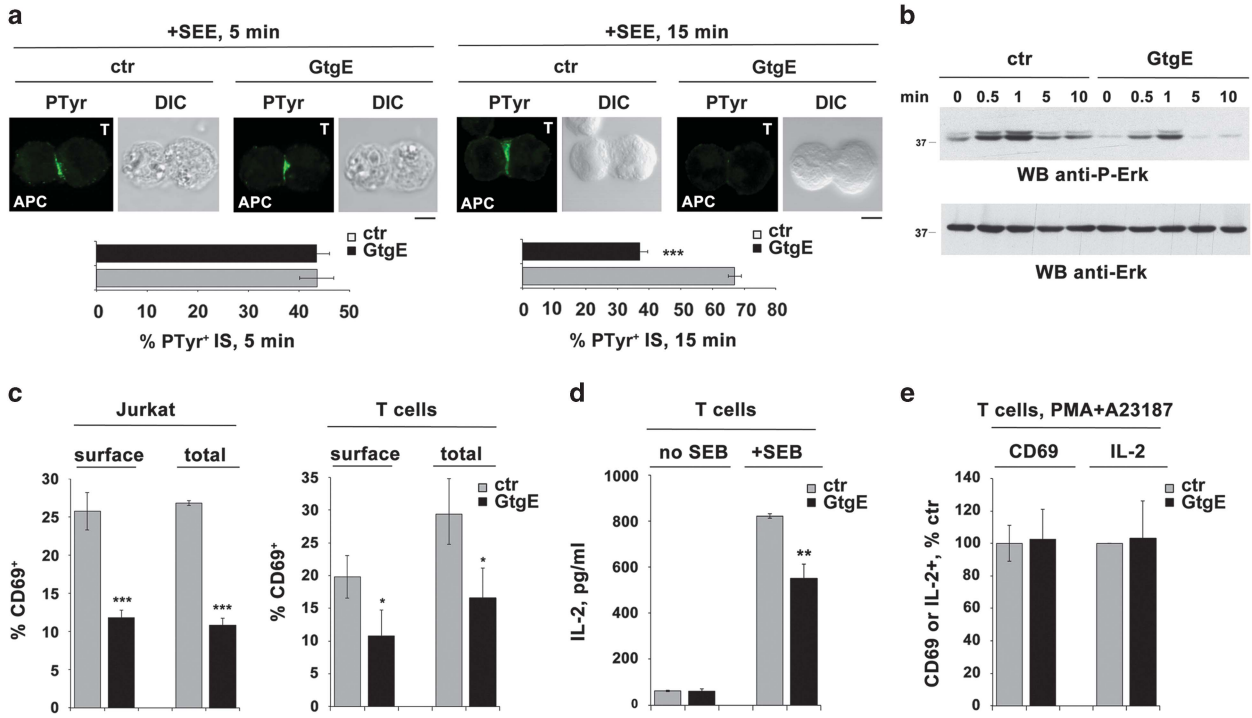

Figure 4 Rab29 is required for T-cell activation. (**a**) Time course immunofluorescence analysis of tyrosine phosphoproteins (PTyr) in conjugates of control and GtgE-expressing Jurkat cells and SEE-pulsed Raji cells (APC). Quantification (%) of conjugates with PTyr staining at the IS 5 min and 15 min after conjugate formation is shown below the representative images. At least 300 cells were analyzed for each marker ($n \geq 3$). Size bar, 5 μm. Error bars, S.D. ***$P < 0.001$. (**b**) Time course immunoblot analysis of Erk phosphorylation in lysates of control or GtgE-expressing Jurkat either unstimulated or activated by TCR cross-linking. The migration of molecular mass markers is indicated ($n = 3$). (**c**) Flow cytometric analysis of surface CD69 in control or GtgE-expressing Jurkat cells (left, $n = 3$) or primary T cells transiently transfected with the GtgE expression construct or empty vector (right, analysis carried out in triplicate on three donors) incubated for 16 h (Jurkat cells) or 30 h (primary T cells) with SAg-loaded Raji B cells (SEE for Jurkat cells, SEB for T cells). Cells were co-stained for CD19 (expressed only by Raji cells) and the analysis was carried out gating on CD19-negative cells. A similar analysis was carried out on permeabilized cells to measure total CD69. The data are expressed as % $CD69^+$ T cells (mean $\pm$ S.D.). (**d**) ELISA quantification of IL-2 in culture supernatants of primary T cells transiently transfected with the GtgE expression construct or empty vector and incubated for 30 h with SEB-loaded Raji B cells. The data are presented as pg/ml (mean $\pm$ S.D.). The analysis was carried out in triplicate on three donors. (**e**) Flow cytometric analysis of CD69 and IL-2 expression in primary T cells transiently transfected with the GtgE expression construct or empty vector and activated using a combination of 50 ng/ml PMA and 100 ng/ml A23187 as a TCR-independent control. The results, which refer to triplicate samples from three donors, are plotted as % $CD69^+$ or $IL\text{-}2^+$ T cells (PMA/A23187-activated T cells transfected with empty vector taken as 100%). ***$P < 0.001$; **$P < 0.01$; *$P < 0.05$

the step controlled by Rab29 in the TCR recycling pathway, we analyzed the localization of the $CD3^+$ compartment in permeabilized control and GtgE-expressing Jurkat cells. Rab29 depletion resulted in impaired polarization of TCR^+ endosomes toward the IS (Figures 5a and c) despite a normal polarization of both the centrosome (Figures 5b and c) and the bulk of early ($Rab5^+$) and recycling ($Rab4^+$, $Rab11^+$) endosomes (Supplementary Figure S4, legend). Tracking TCRs that had been internalized at the plasma membrane in permeabilized conjugates co-stained for γ-tubulin showed that these TCRs were gathered around the centrosome in control cells, while they were dispersed away from the centrosome in GtgE-expressing cells (Figure 5d).

Similar to Rab29-depleted T cells, IFT20-depleted T cells have a defect in TCR recycling to the IS which results from impaired TCR^+ endosome polarization,[14] suggesting that they may participate in the same pathway. We have shown that IFT20 participates early in the pathway by controlling TCR traffic from early to recycling endosomes.[5] Taken together with the ability of Rab29 to colocalize strongly with Rab11 but poorly with Rab5, this indicates that Rab29 acts downstream of IFT20 in the Rab11-dependent recycling pathway. To understand where in the pathway Rab29 maps with respect to Rab11, we asked whether Rab29 depletion could alter the association of recycling TCRs with $Rab11^+$ endosomes. A substantially increased colocalization of internalized TCRs with Rab11 was detected in Rab29-depleted cells (Figure 5e), indicating that Rab29 is required for the transit of recycling TCRs from $Rab11^+$ endosomes to the next step in the pathway.

One possible cause of the inability of recycling TCRs to polarize toward the IS in Rab29-depleted cells is the failure of TCR^+ endosomes to move along the microtubules due to defective coupling to molecular motors, which act as effectors for other Rabs.[22] The ability of Rab29 to interact with the minus-end motor dynein, which is responsible for TCR trafficking to the polarized centrosome during IS assembly,[23] was assessed in co-immunoprecipitation assays. Rab29 was found to constitutively interact with dynein in Jurkat cells (Figure 5f). TCR engagement resulted in its association with dynein in control but not in Rab29-depleted cells (Figure 5g), indicating that Rab29 promotes dynein recruitment to recycling TCRs for their traffic to the polarized centrosome.

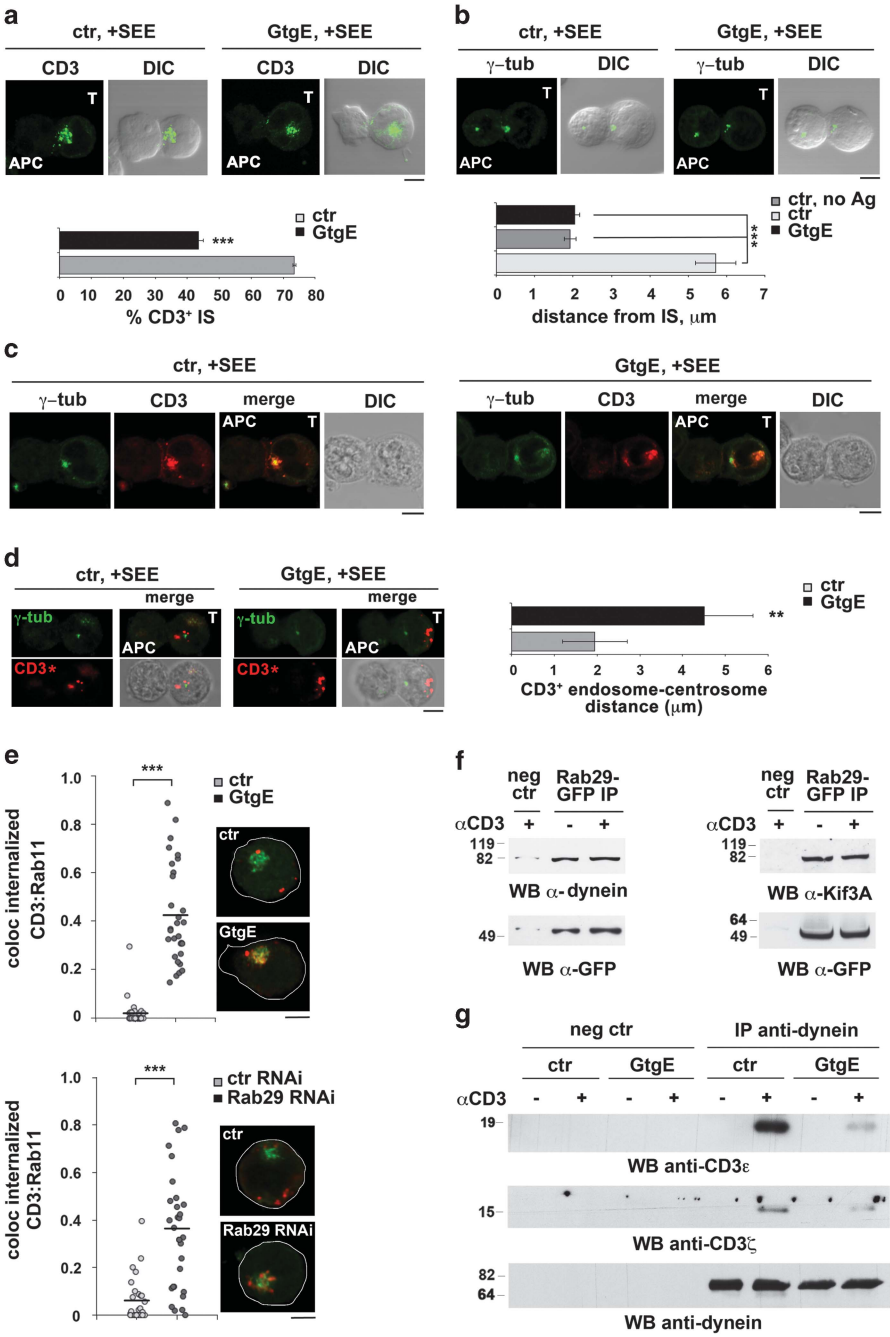

Figure 5 Rab29 is required for TCR recycling downstream of Rab11 by interaction of molecular motors. (**a**) Immunofluorescence analysis of the localization of $CD3^+$ endosomes in conjugates of control or GtgE-expressing Jurkat cells and SEE-pulsed Raji cells (APC). Quantification (%) of conjugates with full polarization of the $CD3^+$ compartment at the IS is shown below the representative images. At least 300 cells were analyzed ($n \geq 3$). (**b**) Immunofluorescence analysis of γ-tubulin localization in conjugates of control or GtgE-expressing Jurkat cells and SEE-pulsed Raji cells (APC). The histograms show the mean distance ± S.D. of the centrosome from the T-cell–APC contact site in conjugates formed with APC in the presence or absence of SEE. At least 300 cells were analyzed ($n \geq 3$). (**c**) Immunofluorescence analysis of $CD3^+$ endosomes (red) in Ag-specific conjugates of control or GtgE-expressing Jurkat cells co-stained for γ-tubulin (green). (**d**) Immunofluorescence analysis of recycling CD3 (CD3*, red) in permeabilized control or GtgE-expressing Jurkat cells conjugated with SEE-pulsed Raji cells (APC). Cells were costained with anti-γ-tubulin mAb (green). The histogram shows the distance (mean ± S.D.) of vesicles containing internalized CD3 (red) from the centrosome (green) in control and GtgE-expressing cells conjugated with SEE-pulsed Raji cells or unpulsed Raji cells (no Ag) used as a negative control. At least 20 cells were analyzed for each sample ($n = 4$). (**e**) Quantification (mean ± S.D.) using Mander's coefficient of the weighted colocalization of the $CD3^+$ vesicles (red) in the $Rab11^+$ compartment (green) in individual medial confocal sections of control or GtgE-expressing Jurkat cells (*top*), or control and Rab29KD Jurkat cells (*bottom*). At least 20 cells for sample were analyzed from three independent experiments. Size bar, 5 μm. Error bars, S.D. $^{***}P < 0.001$; $^{**}P < 0.01$. (**f**) Immunoblot analysis with the indicated antibodies of GFP-specific immunoprecipitates from lysates of GFP-Rab29-expressing Jurkat cells, either unstimulated or activated for 10 min by TCR cross-linking. The blots were carried out on the same filters used in Figure 1f, accounting for the same GFP control blots. (**g**) Immunoblot analysis of dynein-specific immunoprecipitates from lysates of control and GtgE-expressing Jurkat cells, either unstimulated or activated for 10 min by TCR cross-linking. Preclearing controls are included in each blot (neg ctr). Total cell lysates were included in each gel to identify the migration of the proteins tested. All immunoblots shown are representative of three independent experiments

Interestingly, a constitutive interaction of Rab29 was also observed with the plus-end kinesin motor, Kif3A (Figure 5f), suggesting that Rab29 may also participate in the last steps of polarized recycling of endosomal TCRs by favoring their kinesin-dependent movement along the short microtubules connecting the centrosome to the IS membrane.[24]

Rab29 participates in primary cilium assembly. The regulation of polarized TCR recycling to the IS by components of the IFT system that are essential for ciliogenesis[5,14] underscores the similarities between these structures. To understand whether Rab29 is a component of the trafficking machinery responsible for cilium assembly, we extended our analysis to ciliated cells. Real-time PCR analysis of Rab29, Rab32 and Rab38 expression on the ciliated cell lines NIH-3T3 and IMCD showed that they are expressed in these cells, with higher relative levels for Rab29 and Rab32 in NIH3T3 cells, and Rab29 being the most abundant in IMCD cells, similar to T cells (Figure 6a).

Rab29 localized at a vesicular compartment at the base of the cilium in NIH-3T3 or IMCD cells transiently transfected with the GFP-Rab29-encoding construct (Figure 6b). GtgE expression resulted in effective Rab29 depletion (see legend). Similar to T cells, this was reflected by a conversion of the GFP-Rab29 staining from compact to particulate (Figure 6b). No obvious alteration either in the structure of the cis-Golgi, the TGN, or the recycling compartment, or in IFT20 localization, was observed in the absence of Rab29 (Supplementary Figure S5A). Moreover Rab29 depletion did not alter the expression of either Rab GTPases implicated in ciliogenesis (Rab8, Rab11)[21,25] or IFT20, which is essential for ciliary protein trafficking from the Golgi to the basal body (Supplementary Figure S5B).[12] Under these conditions, the number of cells bearing a primary cilium (~70% NIH-3T3; ~30% IMCD) was not affected; however, the ciliary length was significantly shorter in GtgE-expressing cells (Figure 6b). A reduction not only in ciliary length but also in the number of ciliated cells was observed in cells depleted of Rab29 by RNAi (Figure 6c), likely due to the more effective Rab29 depletion compared with GtgE-expressing cells (see legend). The ciliary defect was confirmed by electron microscopy (Figure 7a). An ultrastructural analysis of the cilium showed that the microtubule structure was not altered either in the basal body or in the ciliary axoneme in GtgE-expressing cells (Supplementary Figure S6A). Hence Rab29 participates in ciliogenesis by controlling cilium growth.

To understand whether Rab29 participates in a complex similar to the one observed in T cells, the ability of Rab29 to interact with Rab11, Rab8 and IFT20, or Rab7 used as a negative control was assessed in co-immunoprecipitation experiments on NIH3T3 and IMCD transfectants expressing GFP-Rab29. Rab29 was found to interact with Rab11, Rab8 and IFT20, but not Rab7, in both transfectants (Figure 8a). Moreover, similar to T cells, dynein and Kif3A were found to co-precipitate with Rab29 (Figure 8a) suggesting that Rab29 controls ciliary growth by promoting the transport of endosome-associated ciliary cargo to the base of the cilium. In support of this notion, an EM analysis of NIH-3T3 cells showed that, when compared with cells transfected with empty vector, where abundant vesicles were observed close to or fusing with the periciliary membrane and alar sheets, GtgE-expressing cells had a significantly reduced vesicle enrichment around the ciliary pocket (control cells, 13.7 ± 1.7 vesicles; GtgE-expressing cells, 5.3 ± 1.2) (Figures 7b and c; Supplementary Figure S6B).

To directly assess the role of Rab29 in protein trafficking to the ciliary membrane, we investigated the impact of Rab29 depletion on the localization of *Smoothened*, a receptor that localizes to the ciliary membrane in response to Hedgehog signaling.[26] NIH3T3 and IMCD cells were transiently cotransfected with the GtgE expression construct and a construct encoding GFP-tagged *Smoothened* (Smo-GFP), and the localization of the chimeric protein was analyzed by confocal microscopy. The majority (~90%) of Smo-GFP-expressing cells showed a specific ciliary localization of Smo (Figure 8b), in agreement with the observation that Smo constitutively localizes to the cilium when overexpressed.[27] At variance, a substantial proportion (~70%) of Rab29-depleted cells showed a diffuse cellular distribution of Smo-GFP, with a complete absence in the short cilium (Figure 8b). Similar results were obtained when Rab29 was depleted by RNAi (Figure 8c). At variance, Rab29 depletion did not affect the localization of β1 integrin, which we found to tightly segregate to the cilium (Supplementary Figure S5C). Hence Rab29 is required for Smo trafficking to the ciliary membrane.

Discussion

In *Salmonella*-infected epithelial cells, where its function was initially characterized, Rab29 is recruited to the SCV to promote typhoid toxin transport to the extracellular milieu.[15] Recently, Rab29 has been implicated in retromer-mediated trafficking of the MPR, a receptor that carries newly synthesized lysosomal enzymes to late endosomes and shuttles back to the Golgi, without affecting anterograde transport to the plasma membrane.[18,19] Here we identify a new physiological function for Rab29 as a shared regulator of the trafficking pathways that control receptor recycling and IS assembly in the non-ciliated T cells as well as trafficking to and assembly of the primary cilium in ciliated cells.

Our data indicate that Rab29 controls TCR recycling in the Rab11-dependent route as a complex with IFT20 and Rab8. Rab29 appears to function downstream of IFT20, which associates with Rab5 and is required for TCR trafficking from early endosomes.[5] Rab29 shows indeed a significant colocalization with Rab11 but not with Rab5, suggesting that it is recruited to TCR^+ endosomes after their sorting to recycling endosomes. On the other hand, the finding that recycling TCRs accumulate in $Rab11^+$ endosomes in Rab29-depleted cells indicates that Rab29 participates in the pathway downstream of Rab11.

The interaction of Rab29 with the minus-end microtubule motor dynein, which similar to other Rabs is likely to be indirect,[28,29] suggests a role for this GTPase in coupling TCRs internalized at the plasma membrane to the microtubules emanating from the centrosome. The fact that internalized TCRs accumulate in the $Rab11^+$ pericentrosomal compartment in Rab29-depleted cells undergoing constitutive recycling indicates that Rab29 is dispensable for dynein-dependent trafficking of internalized TCRs to this

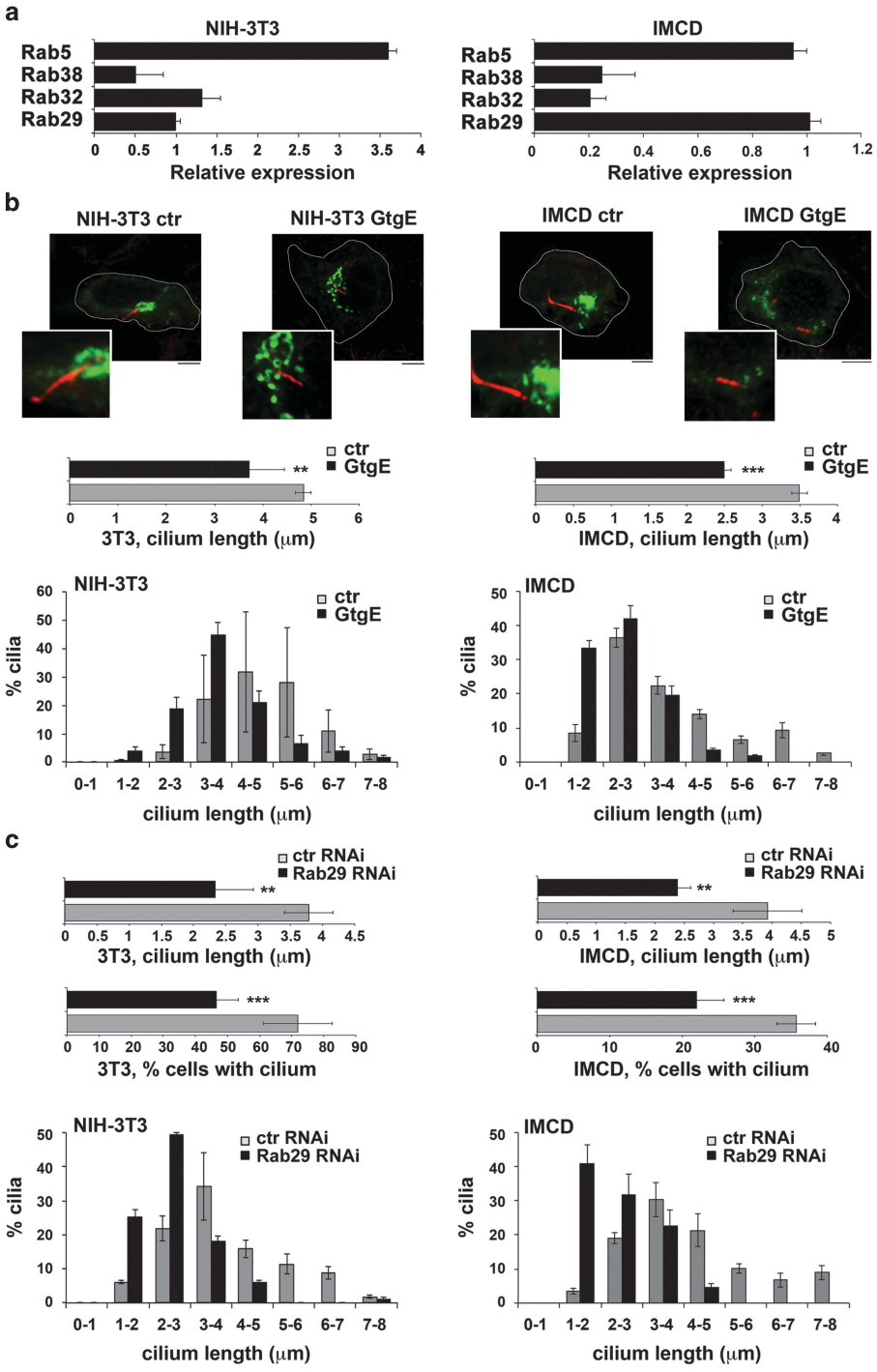

Figure 6 Rab29 is expressed in ciliated cells and is required for primary cilium growth. (**a**) Relative expression of Rab29, Rab32 and Rab38 mRNA in NIH-3T3 and IMCD cells, as determined by real-time RT-PCR. Rab5 was included as an ubiquitous Rab control. The data, determined on triplicate samples using the ddCt method, are expressed using Rab29 as a reference. Error bars, S.D. ($n \geq 3$). (**b**) *Upper*, Immunofluorescence analysis of GFP-tagged Rab29 (green) and acetylated tubulin (red) localization in NIH3T3 (*left*), or IMCD (*right*) cells transiently transfected with a construct encoding GFP-tagged Rab29. The insets in the bottom left corner of the corresponding image are shown at a higher magnification (×2). Size bar, 5 μm. *Middle,* Quantification of ciliary length (μm) in control and GtgE-expressing cells (Rab29 depletion ~ 40% NIH3T3, ~ 30% IMCD). At least 200 cilia in control and GtgE-expressing NIH3T3 cells and 100 cilia in control and GtgE-expressing IMCD cells were analyzed ($n = 3$). *Bottom*, Cilia length distribution, obtained by measuring 200 cilia in control and GtgE-expressing NIH3T3 cells and 100 cilia in control and GtgE-expressing IMCD cells ($n = 3$). The Y axis represents the % of individual cilia with a given length. The X axis represents cilia length (μm). (**c**) *Upper*, Quantification of ciliary length (μm) and proportion of cells bearing a cilium (%) in control and Rab29KD ciliated cells (Rab29 depletion ~ 50% NIH3T3, ~ 40% IMCD). In all, 120 cilia in control and Rab29KD NIH3T3 cells and 90 cilia in control and Rab29 KD IMCD cells were analyzed ($n = 4$). *Bottom*, Cilia length distribution, obtained by measuring 120 cilia in control and Rab29KD NIH3T3 cells and 90 cilia in control and Rab29 KD IMCD cells ($n = 3$). Error bars, S.D. $^{***}P < 0.001$; $^{**}P < 0.01$

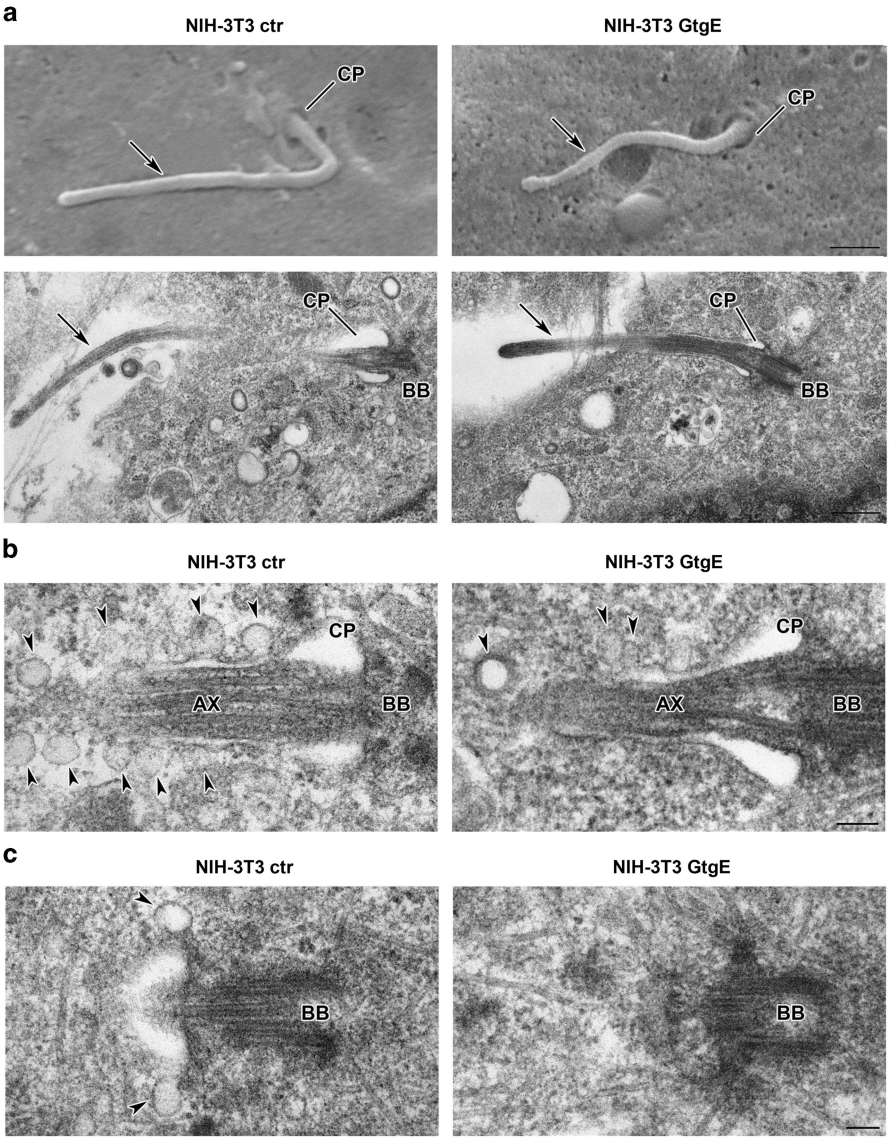

Figure 7 Rab29 deficiency affects the growth of and membrane trafficking to the primary cilium. (**a**) SEM (*upper*) and TEM (*bottom*) analysis of control and GtgE-expressing NIH3T3 cells. The arrows indicate the primary cilium. BB, basal body; CP, ciliary pocket. Size bar, 500 nm. (**b and c**) TEM analysis of control and GtgE-expressing NIH3T3 cells in which the presence of vesicles in the proximity of the periciliary membrane (**b**) as well as of the alar sheets (**c**) is shown. The arrowheads indicate the vesicles. AX, axoneme; BB, basal body; CP, ciliary pocket. Size bar, 100 nm

compartment but is required for their subsequent movement to the centrosome where they can be coupled to kinesin for transport to the plasma membrane. This notion is supported by the dissociation of the TCR^+ endosomes from the centrosome during IS assembly in Rab29-depleted cells, where the centrosome but not the recycling TCRs translocate toward the APC. Taken together with the failure of the TCR to interact with dynein in the absence of Rab29, this result indicates that the function of Rab29 is to couple the $Rab11^+$ endosomes carrying TCR cargo to dynein for their transport to the polarized centrosome, resulting in their correct positioning for IS delivery. It is noteworthy that Rab29 also interacts with Kif3A. Although the centrosome polarizes very close to the IS membrane,[30] recent evidence has highlighted the presence of short microtubules emanating from the polarized centrosome and directed toward the IS membrane in cytotoxic T cells, on which transport is ensured by kinesin 1/Kif5b.[24] Our finding that Rab29 interacts with Kif3A suggests the possibility that it may further participate in the pathway by coupling the TCR^+ endosomes that have reached the centrosome to these short microtubules for their kinesin-dependent transport to the IS.

We have recently reported that IFT20 regulates TCR and TfR, but not CXCR4 recycling.[5] Surprisingly, Rab29, while participating in TCR recycling, appears required for CXCR4 recycling but dispensable for TfR recycling. Moreover, Rab29 depletion does not affect the IS polarization of the bulk of recycling endosomes. The results highlight the existence of multiple pathways assembled by combining individual regulators/effectors to control recycling of specific receptors in T cells, with Rab29 regulating only a subset. More generally, they support the emerging notion that different subpopulations of recycling endosomes, while participating in the pathways

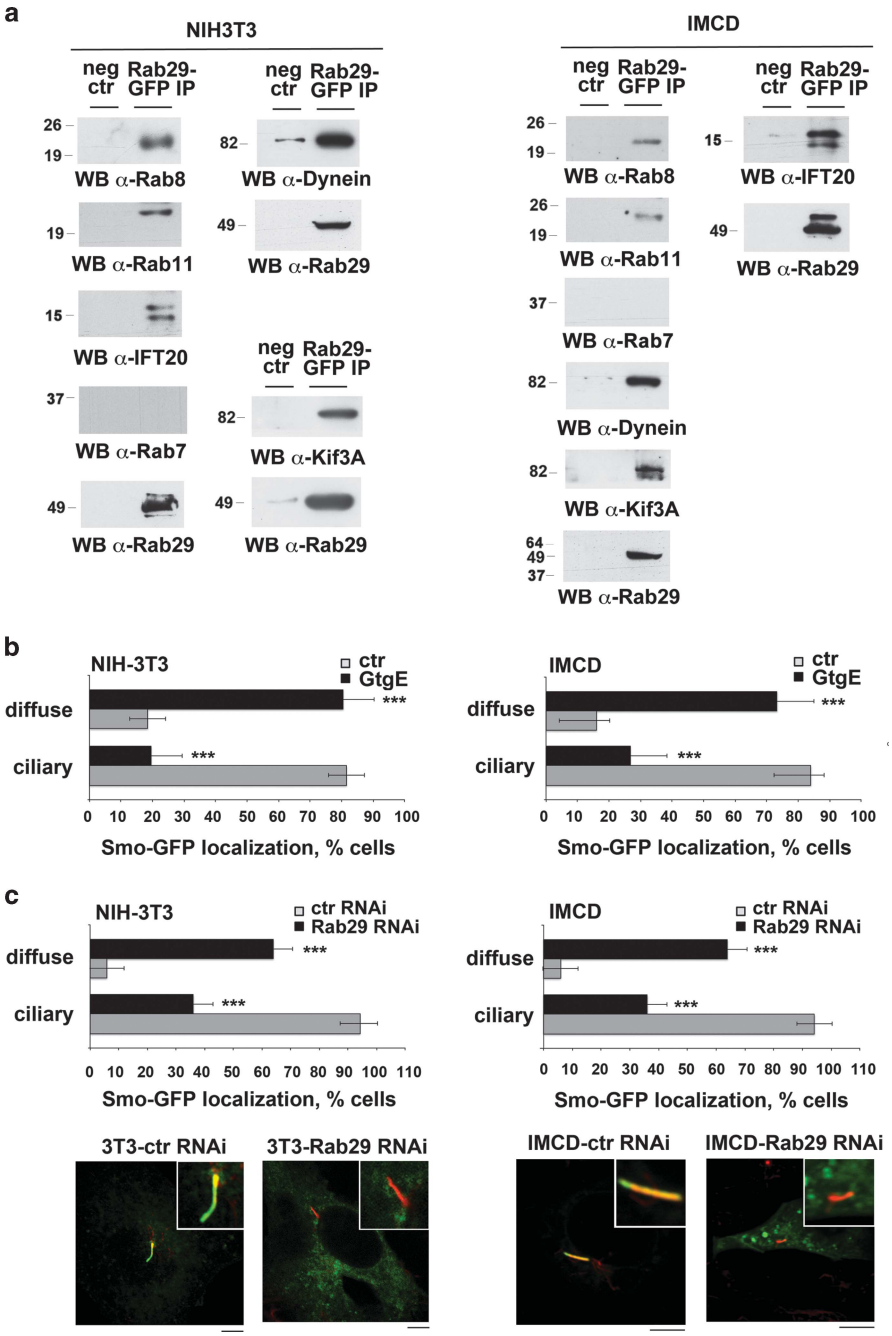

Figure 8 Rab29 forms a complex that includes Rab8, Rab11 and the dynein and kinesin motors in ciliated cells and is required for Smo trafficking to the cilium. (**a**) Immunoblot analysis of GFP-tagged Rab29-specific immunoprecipitates from lysates of ciliated cells. Preclearing controls are included in each blot (neg ctr). Total cell lysates were included in each gel to identify the migration of the proteins tested. The immunoblots shown are representative of ≥ 3 independent experiments. (**b**) Quantification (%, mean $\pm$ S.D.) of cells with diffuse or ciliary localization of Smo-GFP, in control and GtgE-expressing NIH3T3 and IMCD transfectants ($\geq$20 cells/sample, $n=3$). (**c**) *Upper*, Quantification (%, mean $\pm$ S.D.) of cells with diffuse or ciliary localization of Smo-GFP in control and Rab29KD NIH3T3 and IMCD cells. The data are expressed as mean $\pm$ S.D. ($\geq$20 cells/sample, $n=3$). *Bottom*, Immunofluorescence analysis of Smo-GFP (green) and acetylated tubulin (red) localization in NIH-3T3 or IMCD cells transiently co-transfected with a construct encoding Smo-GFP and with Rab29 esiRNAs. The insets in the upper right corner of the corresponding image are shown at a higher magnification (x2.5). Size bar, 5 μm. Error bars, S.D. ***$P<0.001$

regulated by Rab4 and Rab11, are responsible for trafficking specific receptor cargo, allowing specificity to be achieved within these pathway.

Remarkably, our data reveal a role for Rab29 as a novel regulator of ciliogenesis. The ciliary defect appears limited to growth, as no ultrastructural alteration could be detected. Moreover, at variance with the TGN fragmentation observed by Wang *et al.*[18] when Rab29 expression or function was disrupted in epithelial cells, but consistent with the finding obtained on neurons by McLeod *et al.*,[19] no gross morphological alterations in either the cis- or the trans-Golgi were observed in either NIH-3T3 or IMCD cells. Similar to T cells,

Rab29 interacts in these cells with dynein and kinesin as well as with Rab8, which is required for protein transport into the cilium[21] and Rab11, which is responsible for the transport of the Rab8 GEF, Rabin8, to the pericentrosomal compartment where it recruits Rab8 to the BBSome.[21,25] Moreover Rab29 interacts with IFT20, which not only participates in intraflagellar trasport but is also implicated in sorting ciliary receptors such as rhodopsin at the level of the Golgi apparatus.[31] Since Rab29 localizes at the base of the cilium but not in the cilium itself, at variance with Rab8 and IFT20, this suggests that it may promote ciliary growth by assisting the microtubule-dependent transport of endosomal cargo destined for the cilium to the basal body for its subsequent Rab8- and IFT20-dependent ciliary transport. This notion is supported by the failure of Smo to localize to the cilium in the absence of Rab29. It is noteworthy that the outcome of Rab29 deficiency on the ciliary localization of Smo is more pronounced when compared with its effect on ciliary growth. Taken together with the lack of effect of Rab29 depletion of the membrane localization of β1 integrin, that had been shown to associate with the cilium in chondrocytes[32] and that we found to be restricted to the cilium in epithelial cells, this suggests that, similar to T cells, Rab29 controls the traffic of a subset of proteins to the ciliary membrane. The identification of Rab29 as a component of the vesicular trafficking pathway that controls the extension of the primary cilium as well as the assembly of the IS in the non-ciliated T cell not only provides insights into the mechanisms that control ciliogenesis, but also strongly underscores the homologies between these two structures, as also supported by a recent report showing the Sonic hedgehog signaling, which is orchestrated by the primary cilium, is essential for IS assembly in cytotoxic T cells.[33]

Our data may have relevance to our understanding of *Salmonella* pathogenesis. In addition to indirectly modulating T-cell activation,[34] *Salmonella* can directly suppress T-cell responses by contact-dependent downmodulation of TCR expression[35] as well as by limiting the availability of L-asparagine.[36] Moreover, both CD4 and CD8 T cells have been shown to internalize *S.* thyphimurium in infected mice.[37] The implication of Rab29 in IS assembly and T-cell activation suggests a potential novel target for immune evasion by *Salmonella* involving the protease GtgE. By preventing the delivery to the IS of endosomal TCRs, which requires Rab29, in infected T cells, GtgE would be expected to effectively suppress the long-lasting signaling required for T-cell activation.

Materials and Methods

Cells, plasmids, antibodies and reagents. Cells included Jurkat T cells, Raji B cells, normal peripheral blood T cells, NIH3T3 murine fibroblasts and IMCD murine kidney cells. Polyclonal anti-IFT20 antibodies were previously described.[38] IgG from OKT3 (anti-human CD3ε, IgG2) hybridoma supernatants was purified using Mabtrap (Amersham Biosciences, Inc., Piscataway, NJ, USA) and titrated by flow cytometry. Anti-TfR mAb (hybridoma OKT9) was generously provided by A Alcover, anti-CXCR4 antibodies by J Hoxie, Leukosite and the MRC AIDS Reagent Project. All primary commercial antibodies used in this work are listed in Supplementary Table S1, together with information about the dilutions used for immunofluorescence and immunoblotting. Unlabeled secondary antibodies were from Cappel (ICN Pharmaceuticals Inc., Costa Mesa, CA, USA), secondary peroxidase-labeled antibodies from Amersham Biosciences, Alexa Fluor 488- and 555-labeled secondary Abs from Molecular Probes (Invitrogen, Eugene, OR, USA), PE-conjugated anti-mouse Ig from eBiosciences (San Diego, CA, USA).

The endoribonuclease-prepared siRNA used to silence Rab29 in human (EHU025091) and mouse (EMU031981) cells, as well as unrelated control RLUC esiRNA (EHURLUC) were purchased from Sigma-Aldrich (The Woodlands, TX, USA). The respective sequences are listed in Supplementary Table S2.

Plasmids included pcDNA3.1 (Invitrogen V790-20), pRK5-GtgE,[15] pEGFP-Rab29,[15] pEGFP-mouse Smoothened (pEGFP-mSmo) (Addgene plasmid #25395)[39] and pJAF2.13.[12] pRK5-GtgE was digested with XbaI-BamHI and the GtgE insert was subcloned into the corresponding sites of pcDNA3.1.

Staphylococcal enterotoxins E (SEE) and B (SEB) were purchased from Toxin Technology (Sarasota, FL, USA), poly-L-lysine and protease inhibitors from Sigma-Aldrich.

Transfections and RNA interference. Jurkat cell lines stably transfected with pcDNA3.1 (empty vector, ctr) or pcDNA3.1-GtgE (GtgE) were generated as described.[40] GtgE cells were routinely checked for Rab29 depletion by immunoblot. A Jurkat cell line stably transfected with a GFP-tagged Rab29 construct was also generated using pEGFP-Rab29. Human Rab29-specific esiRNAs and unrelated control esiRNA (Supplementary Table S2) were transfected by electroporation and assays carried out after 48 h. Primary T cells were transiently transfected by nucleofection with pcDNA3.1 and pcDNA3.1-GtgE, or Rab29-specific esiRNAs and unrelated control esiRNA, using the Amaxa nucleofector device (Amaxa Biosystems, Cologne, Germany) and the conditions for T-cell transfection recommended by the manufacturer. Cells were analyzed 24 h post transfection. Cell viability was measured by flow cytometric analysis following cell staining with FITC-labeled annexin V and propidium iodide (Annexin V-FITC Apoptosis Detection Kit, eBioscience) under non-permabilizing conditions.

Transient transfections of NIH-3T3 and IMCD cells with pcDNA3.1, pcDNA3.1-GtgE, pEGFP-Rab29, pEGFP-mSmo and pJAF2.13 were performed by using Turbofectamine (ThermoScientific, Bonn, Germany) and assays carried out after 24 and 48 h. Murine Rab29-specific esiRNAs and unrelated control esiRNA (Supplementary Table S2) were transfected by Lipofectamine RNAiMAX Transfection Reagent (Life Technologies, Monza, Italy) and assays carried out after 48 h. Transient co-transfection of murine Rab29-specific esiRNA and pEGFP-mSmo was performed by using dharmaFECT Duo Transfection Reagent (ThermoScientific) and assays were carried out after 48 h.

Conjugate formation, T-cell activation assays. Conjugates between Jurkat or normal T cells and superantigen (SAg)-pulsed Raji B cells were carried out as previously decribed.[14] SEE was used for Jurkat cells, which express a TCR Vβ that specifically recognizes this SAg, while SEB was used for normal T cells, as this SAg covers a wider proportion of TCR Vβ repertoire compared to SEE. Analyzes were carried out 15 min after conjugate formation, with the exception of the analyses shown in Figure 4a, which included a shorter time (5 min). Conjugates between T cells and unpulsed B cells, where no IS forms at the interface of the cell pairs, were used as negative controls.

T-cell activation following incubation of Jurkat cells (16 h) or primary T cells (30 h) with Raji cells in the presence or absence of SAg was quantitated by flow cytometric analysis of surface CD69, excluding from the analysis the $CD19^+$ Raji cells. To rule out an effect of Rab29 depletion on CD69 transport to the cell surface, CD69 was also quantitated in cells permeabilized using the kit Cytofix/cytoperm plus (BD Biosciences, San Jose, CA, USA). Flow cytometric analysis of IL-2 expression was carried out by intracellular staining with FITC-labeled rat anti-human IL-2 (BD Biosciences). Alternatively, IL-2 was measured in culture supernatants using the Human IL-2 Ready-Set-Go! ELISA kit from eBioscience. Isotype controls (BD Biosciences) were used for all FACS experiments involving directly labeled antibodies, while fluorochrome-conjugated secondary antibodies were used as controls for experiments involving unlabeled primary antibodies.

Flow cytometry and immunofluorescence analysis of receptor recycling. Flow cytometric and immunofluorescence analysis of receptor recycling was carried out as previously described.[5] Receptor recycling was quantitated by flow cytometry. Cells were equilibrated for 30 min at 37 °C in RPMI 1% BSA, then incubated 30 min on ice with saturating concentrations (determined by flow cytometry) of receptor-specific mAb to allow binding, washed with cold PBS and shifted to 37 °C for 15 (TfR) or 60 min (TCR, CXCR4) to allow internalization of receptor–mAb complexes. Cells were acid-stripped to remove residual surface-bound mAb (30 s at RT in 100 mM glycine, 100 mM NaCl, pH 2.5), washed and

incubated at 37 °C to allow recycling of receptor–mAb complexes. Receptor–mAb complexes that had recycled to the cell surface were measured by labeling with fluorochrome-labeled secondary Ig. Recycling was calculated as % of the internalized receptors that had recycled to the cell surface as described,[41] calculated using the formula

$$x_t = \frac{(MFI_t - MFI_s)}{(MFI_{max} - MFI_s) - (MFI_n - MFI_s)} \times 100$$

where MFI_t is the MFI at time '*t*', MFI_s the MFI after acid-stripping of surface-bound mAb, MFI_{max} the MFI after incubation on ice with receptor-specific mAb, MFI_n the MFI after receptor–mAb complexes internalization.

To analyze vesicles containing internalized receptors by immunofluorescence cells were equilibrated as above, then incubated with saturating concentrations of mAb specific for each receptor at 37 °C for 2 h. Cells were washed to remove excess mAb, allowed to adhere for 15 min on poly-L-lysine-coated wells of diagnostic microscope slides (Erie Scientific Company, Lexington, MA, USA), fixed in 4% paraformaldehyde for 15 min at RT and permeabilized in PBS 0.01% Triton X-100 for 30 min at RT. Internalized receptor–mAb complexes were labeled using fluorochrome-labeled secondary Ig and visualized by confocal microscopy. The number of vesicles positive for each receptor was determined in individual medial confocal sections using ImageJ ('analyze particles' function) to identify and count objects, setting as lowest limit 0.005 μm^2 and excluding from the analysis the compact pericentrosomal compartment where objects could not be discriminated.

To analyze TCR, TfR or CXCR4 recycling at the IS, T cells were equilibrated as above, then incubated with saturating concentrations of mAb specific for each receptor at 37 °C for 2 h. Residual surface-bound mAb was removed by acid stripping. Cells were then mixed with SEE (SEB)-pulsed Raji cells, incubated 15 min at 37 °C, plated on poly-L-lysine-coated wells and fixed and permeabilized by immersion in methanol for 10 min at − 20 °C, or analyzed under non-permeabilizing conditions after fixation in 4% paraformaldehyde to specifically track receptors that had recycled to the IS membrane.

Immunofluorescence microscopy, colocalization analyses, electron microscopy. Following fixation, samples were washed 5 min in PBS and incubated with primary antibodies overnight at 4 °C or 1 h at RT. After washing in PBS, samples were incubated for 1 h at RT with Alexa Fluor 488- and 555-labeled secondary antibodies.

Confocal microscopy was carried out on a Zeiss LSM700 (Oberkochen, Germany) using a ×63 objective. Z series of optical sections was performed at 0.5 μm increments. Images were acquired with pinholes opened to obtain 0.8-μm-thick sections. Detectors were set to detect an optimal signal below the saturation limits. Images were processed with Zen 2009 image software (Carl Zeiss, Jena, Germany).

The colocalization analyses were carried out on the GFP-Rab29 stable Jurkat transfectant as well as on normal T cells transiently transfected with the GFP-tagged Rab29 construct. The quantitative colocalization analysis of GFP-Rab29 with other Rabs, GM130, TGN46 and IFT20 was performed on median optical sections using ImageJ and JACoP plug-in to determine Manders' coefficient M_1,[42] which represents the percentage of GFP-Rab29 pixels (green channel) that overlaps Rab4, Rab5, Rab8, Rab11, GM130, TGN46 or IFT20 pixels (red channel) (0 = no colocalization; 1 = 100% colocalization). The quantitative colocalization analysis of internalized CD3 and GFP-Rab29 or Rab11 was assessed as above, analyzing the percentage of CD3 pixels (red channel) that overlap with GFP pixels (green signal). The distance of vesicles containing internalized CD3 from the centrosome was measured using ImageJ. Centrosome polarization to the IS, assessed as the reduction in the distance of the centrosome from the APC contact site in T cells exposed to SEE-loaded versus unloaded APC,[43] was measured using ImageJ. Scoring of conjugates for polarized receptor recycling to the IS was based on the presence of staining solely at the T-cell contact with the APC, the remaining membrane being negative.

The length of cilia was measured using ImageJ on NIH3T3 and IMCD cells grown to 70–90% confluency and serum-starved for 24–48 h, followed by fixation and permeabilization by immersion in methanol for 10 min at − 20 °C and staining with an anti-acetylated tubulin mAb.

Electron microscopy and colocalization analyses. Cells were plated on coverslips, fixed overnight at 4 °C in 2.5% glutaraldehyde in PBS, post-fixed for 1 h at 4 °C in 1% osmium tetraoxide in PBS, and then dehydrated in a graded series of ethanol. For Scanning Electron Microscope (SEM) observations, samples were critical-point dried in a Balzers CPD 030 apparatus (Balzers, Liechtenstein, Europe), mounted on aluminium stubs, gold-coated in a Balzers MED 010 sputtering device (Balzers), and observed with a Philips XL20 scanning electron microscope (PHILIPS/FEI, Eindhoven, Holland) operating at 10 kV. For Transmission Electron Microscope (TEM) observations, samples were embedded in a mixture of Epon-Araldite resin and polymerized for 48 h at 60 °C. Coverslips were separated from the resin after a quick immersion in liquid nitrogen. Ultrathin sections (65–60 nm) were obtained with a Reichert ultramicrotome equipped with a diamond knife, collected with formvar-coated copper grids, and stained with uranyl acetate and lead citrate. Preparations were observed with a FEI Tecnai G2 Spirit transmission electron microscope (FEI, Hillsboro, OR, USA) operating at 100 kV. To analyze vesicle enrichment in cilia of control- and GtgE-expressing cells, vesicles were counted in a 1.5 μm × 1.5 μm area along the ciliary pocket starting from the basal body.

Cell activation, protein immunoprecipitation and immunoblotting. Activations of Jurkat cells by antibody-mediated TCR ligation were performed as previously described[5] by incubating Jurkat cells (5×10^7/sample for immunoprecipitation experiments on the ctr/GtgE or ctr/GFP-Rab29 transfectants; 3×10^6/sample for immunoblot experiments on total cell lysates), resuspended in RPMI (200 μl and 50 μl, respectively) with saturating concentrations of anti-CD3 mAb (determined by flow cytometry for each OKT3 batch) and 50 μg/ml goat anti-mouse Ig for 10 min at 37 °C. For immunoprecipitation experiments on NIH3T3 and IMCD cells, 5×10^7/sample for ctr/GFP-Rab29 transfectants was used. Cells were pelleted, washed twice in ice-cold PBS and lysed in 0.5% Triton X-100 in 20 mM Tris-HCl (pH 8.0), 150 mM NaCl in the presence of protease inhibitors (Sigma-Aldrich) (500 μl for Jurkat cells or 1 ml for NIH3T3 and IMCD cells for immunoprecipitations, 50 μl for immunoblot analysis of total cell lysates). Post-nuclear supernatants (2 mg/sample for the ctr/GtgE samples and for the GFP-Rab29 transfectants; quantification carried out using the BCA Assay kit from Pierce, Rockford, IL, USA) were immunoprecipitated for 2 h using, depending on the antibodies to be used for the subsequent immunoblot analysis, either 2 μg mouse anti-GFP mAb (Life Technologies) or 2 μg rabbit anti-GFP polyclonal antibodies (Life Technologies), or 2 μg rabbit anti-Rab8 (Cell Signalling, Danvers, MA, USA) or 2 μg mouse anti-dynein mAb (Millipore), and 3 mg/sample protein-A-Sepharose (PAS) (Amersham). Before immunoprecipitation, post-nuclear supernatants were precleared for 1 h with the same amount of PAS. PAS–antibody complexes as well as PAS controls were pelleted, washed 4× with 1 ml TBS-Tween 0.02%, then resuspended in 15 μl Laemmli buffer, boiled for 5 min and subjected to SDS-PAGE. Under these conditions no TCR/CD3 pulldown by the activating anti-CD3 mAb was detectable (Supplementary Figure S7, left; see also Supplementary Figure S1[5]). All gels included a fraction of the lysates used for the IPs (50 μg/sample). Specificity controls for the immunoprecipitation experiments are shown in Supplementary Figure S5B both for Jurkat cells and for NIH-3T3 cells.

Immunoblotting was carried out using peroxidase-labeled secondary Ig and a chemiluminescence detection kit (Pierce). Stripping was carried out by using ReBlot Plus Mild Antibody Stripping Solution, 10× (Chemicon, Darmstadt, Germany). Blots were scanned using a laser densitometer (Duoscan T2500; Agfa, Milan, Italy) and quantified using ImageJ 1.46r (National Institutes of Health, USA).

RNA purification, real-time PCR. RNA was extracted from Jurkat, primary human peripheral blood T cells, NIH3T3 and IMCD cells and retrotranscribed as described.[44] Real-time PCR was performed in triplicate on each cDNA on 96-well optical PCR plates (Sarstedt AG, Nümbrecht, Germany) as described.[45] Transcript levels were normalized to hHPRT1 or mGAPDH, used as housekeeping genes. The primers used to amplify the cDNA fragments corresponding to human and murine transcripts are listed in Supplementary Table S3.

Statistical analysis. Mean values, standard deviation values and Student's *t* test (unpaired) were calculated using the Microsoft Excel application. A *P*-value of < 0.05 was considered as statistically significant.

Conflict of Interest

The authors declare no conflict of interest.

Acknowledgements. We wish to thank Jorge Galán, Gregory Pazour, Derek Toomre, Giuliano Callaini, Joel Rosenbaum, Alessandra Boletta and Francesco Blasi for generously providing reagents and for productive discussions,

and Sonia Grassini for technical assistance. The work was carried out with the financial support of Telethon (GGP11021) and AIRC.

1. Geisler C. TCR trafficking in resting and stimulated T cells. *Crit Rev Immunol* 2004; **24**: 67–86.
2. Das V, Nal B, Dujeancourt A, Thoulouze MI, Galli T, Roux P *et al.* Activation-induced polarized recycling targets T cell antigen receptors to the immunological synapse; involvement of SNARE complexes. *Immunity* 2004; **20**: 577–588.
3. Iezzi G, Karjalainen K, Lanzavecchia A. The duration of antigenic stimulation determines the fate of naive and effector T cells. *Immunity* 1998; **8**: 89–95.
4. Batista A, Millán J, Mittelbrunn M, Sánchez-Madrid F, Alonso MA. Recruitment of transferrin receptor to immunological synapse in response to TCR engagement. *J Immunol* 2004; **172**: 6709–6714.
5. Finetti F, Patrussi L, Masi G, Onnis A, Galgano D, Lucherini OM *et al.* Immune synapse targeting of specific recycling receptors by the intraflagellar transport system. *J Cell Sci* 2014; **127**: 1924–1937.
6. Bonello G, Blanchard N, Montoya MC, Aguado E, Langlet C, He HT *et al.* Dynamic recruitment of the adaptor protein LAT: LAT exists in two distinct intracellular pools and controls its own recruitment. *J Cell Sci* 2004; **117**: 1009–1016.
7. Ehrlich LI, Ebert PJ, Krummel MF, Weiss A, Davis MM. Dynamics of p56lck translocation to the T cell immunological synapse following agonist and antagonist stimulation. *Immunity* 2002; **17**: 809–822.
8. Hutagalung AH, Novick PJ. Role of Rab GTPases in membrane traffic and cell physiology. *Physiol Rev* 2011; **91**: 119–149.
9. Patino-Lopez G, Dong X, Ben-Aissa K, Bernot KM, Itoh T, Fukuda M *et al.* Rab35 and its GAP EPI64C in T cells regulate receptor recycling and immunological synapse formation. *Biol Chem* 2008; **283**: 18323–18330.
10. Gomez DS, Billadeau DD. A FAM21-containing WASH complex regulates retromer-dependent sorting. *Dev Cell* 2009; **17**: 699–711.
11. Soares H, Henriques R, Sachse M, Ventimiglia L, Alonso MA, Zimmer C *et al.* Regulated vesicle fusion generates signaling nanoterritories that control T cell activation at the immunological synapse. *J Exp Med* 2013; **210**: 2415–2433.
12. Follit JA, Tuft RA, Fogarty KE, Pazour GJ. The intraflagellar transport protein IFT20 is associated with the Golgi complex and is required for cilia assembly. *Mol Biol Cell* 2006; **17**: 3781–3792.
13. Pedersen LB, Rosenbaum JL. Intraflagellar transport (IFT) role in ciliary assembly, resorption and signalling. *Curr Top Dev Biol* 2008; **85**: 23–61.
14. Finetti F, Paccani SR, Riparbelli MG, Giacomello E, Perinetti G, Pazour GJ *et al.* Intraflagellar transport is required for polarized recycling of the TCR/CD3 complex to the immune synapse. *Nat Cell Biol* 2009; **11**: 1332–1349.
15. Spanò S, Liu X, Galán JE. Proteolytic targeting of Rab29 by an effector protein distinguishes the intracellular compartments of human-adapted and broad-host Salmonella. *Proc Natl Acad Sci USA* 2011; **108**: 18418–18423.
16. Spanò S, Galán JE. A Rab32-dependent pathway contributes to Salmonella typhi host restriction. *Science* 2012; **338**: 960–963.
17. Wasmeier C, Romao M, Plowright L, Bennett DC, Raposo G, Seabra MC. Rab38 and Rab32 control post-Golgi trafficking of melanogenic enzymes. *J Cell Biol* 2006; **175**: 271–281.
18. Wang S, Ma Z, Xu X, Wang Z, Sun L, Zhou Y *et al.* A role of Rab29 in the integrity of the trans-Golgi network and retrograde trafficking of mannose-6-phosphate receptor. *PLoS ONE* 2014; **9**: e96242.
19. MacLeod DA, Rhinn H, Kuwahara T, Zolin A, Di Paolo G, McCabe BD *et al.* RAB7L1 interacts with LRRK2 to modify intraneuronal protein sorting and Parkinson's disease risk. *Neuron* 2013; **77**: 425–439.
20. Smith AC, Heo WD, Braun V, Jiang X, Macrae C, Casanova JE *et al.* A network of Rab GTPases controls phagosome maturation and is modulated by *Salmonella enterica* serovar Typhimurium. *J Cell Biol* 2007; **176**: 263–268.
21. Nachury MV, Loktev AV, Zhang Q, Westlake CJ, Peränen J, Merdes A *et al.* A core complex of BBS proteins cooperates with the GTPase Rab8 to promote ciliary membrane biogenesis. *Cell* 2007; **129**: 1201–1213.
22. Jordens I, Marsman M, Kuijl C, Neefjes J, Hehnly H. Rab proteins, connecting transport and vesicle fusion. *Traffic* 2005; **6**: 1070–1077.
23. Martín-Cófreces NB, Robles-Valero J, Cabrero JR, Mittelbrunn M, Gordón-Alonso M, Sung CH *et al.* MTOC translocation modulates IS formation and controls sustained T cell signaling. *J Cell Biol* 2008; **182**: 951–962.
24. Kurowska M, Goudin N, Nehme NT, Court M, Garin J, Fischer A *et al.* Terminal transport of lytic granules to the immune synapse is mediated by the kinesin-1/Slp3/Rab27a complex. *Blood* 2012; **119**: 3879–3889.
25. Westlake CJ, Baye LM, Nachury MV, Wright KJ, Ervin KE, Phu L *et al.* Primary cilia membrane assembly is initiated by Rab11 and transport protein particle II (TRAPPII) complex-dependent trafficking of Rabin8 to the centrosome. *Proc Natl Acad Sci USA* 2011; **108**: 2759–2764.
26. Wong SY, Reiter JF. The primary cilium at the crossroads of mammalian hedgehog signaling. *Curr Top Dev Biol* 2008; **85**: 225–260.
27. Wu VM, Chen SC, Arkin MR, Reiter JF. Small molecule inhibitors of Smoothened ciliary localization and ciliogenesis. *Proc Natl Acad Sci USA* 2012; **109**: 13644–13649.
28. Schonteich E, Wilson GM, Burden J, Hopkins CR, Anderson K, Goldenring JR *et al.* The Rip11/Rab11-FIP5 and kinesin II complex regulates endocytic protein recycling. *J Cell Sci* 2008; **121**: 3824–3833.
29. Horgan CP, Hanscom SR, Jolly RS, Futter CE, McCaffrey MW. Rab11-FIP3 links the Rab11 GTPase and cytoplasmic dynein to mediate transport to the endosomal-recycling compartment. *J Cell Sci* 2010; **123**: 181–191.
30. Stinchcombe JC, Majorovits E, Bossi G, Fuller S, Griffiths GM. Centrosome polarization delivers secretory granules to the immunological synapse. *Nature* 2006; **443**: 462–465.
31. Keady BT, Le YZ, Pazour GJ. IFT20 is required for opsin trafficking and photoreceptor outer segment development. *Mol Biol Cell* 2011; **22**: 921–930.
32. McGlashan SR, Jensen CS, Poole CA. Localization of extracellular matrix receptors on the chondrocyte primary cilium. *J Histo Histochem* 2006; **54**: 1005–1014.
33. de la Roche M, Ritter AT, Angus KL, Dinsmore C, Earnshaw CH, Reiter JF *et al.* Hedgehog signaling controls T cell killing at the immunological synapse. *Science* 2013; **342**: 1247–1250.
34. Kalupahana RS, Mastroeni P, Maskell D, Blacklaws BA. Activation of murine dendritic cells and macrophages induced by Salmonella enterica serovar Typhimurium. *Immunology* 2005; **115**: 462–472.
35. van der Velden AW, Dougherty JT, Starnbach MN. Down-modulation of TCR expression by Salmonella enterica serovar Typhimurium. *J Immunol* 2008; **180**: 5569–5574.
36. Kullas AL, McClelland M, Yang HJ, Tam JW, Torres A, Porwollik S *et al.* L-asparaginase II produced by Salmonella typhimurium inhibits T cell responses and mediates virulence. *Cell Host Microbe* 2012; **12**: 791–798.
37. Geddes K, Cruz F, Heffron F. Analysis of cells targeted by Salmonella type III secretion in vivo. *PLoS Pathog* 2007; **3**: e196.
38. Pazour GJ, Baker SA, Deane JA, Cole DG, Dickert BL, Rosenbaum JL *et al.* The intraflagellar transport protein, IFT88, is essential for vertebrate photoreceptor assembly and maintenance. *J Cell Biol* 2002; **157**: 103–113.
39. Chen JK, Taipale J, Cooper MK, Beachy PA. Inhibition of Hedgehog signaling by direct binding of cyclopamine to Smoothened. *Genes Dev* 2002; **16**: 2743–2748.
40. Pacini S, Pellegrini M, Migliaccio E, Patrussi L, Ulivieri C, Ventura A *et al.* p66SHC promotes apoptosis and antagonizes mitogenic signaling in T cells. *Mol Cell Biol* 2004; **24**: 1747–1757.
41. Margadant C, Kreft M, de Groot DJ, Norman JC, Sonnenberg A. Distinct roles of talin and kindlin in regulating integrin alpha5beta1 function and trafficking. *Curr Biol* 2012; **22**: 1554–1563.
42. Manders EM, Stap J, Brakenhoff GJ, van Driel R, Aten JA. Dynamics of three-dimensional replication patterns during the S-phase, analysed by double labelling of DNA and confocal microscopy. *J Cell Sci* 1992; **103**: 857–862.
43. Esquerré M, Tauzin B, Guiraud M, Müller S, Saoudi A, Valitutti S. Human regulatory T cells inhibit polarization of T helper cells toward antigen-presenting cells via a TGF-beta-dependent mechanism. *Proc Natl Acad Sci USA* 2008; **105**: 2550.
44. Patrussi L, Ulivieri C, Lucherini OM, Paccani SR, Gamberucci A, Lanfrancone L *et al.* p52Shc is required for CXCR4-dependent signaling and chemotaxis in T cells. *Blood* 2007; **110**: 1730–1738.
45. Capitani N, Patrussi L, Trentin L, Lucherini OM, Cannizzaro E, Migliaccio E *et al.* S1P1 expression is controlled by the pro-oxidant activity of p66Shc and is impaired in B-CLL patients with unfavorable prognosis. *Blood* 2012; **120**: 4391–4399.

Supplementary Information accompanies this paper on Cell Death and Differentiation website (http://www.nature.com/cdd)